Ionics (2009) 15:405–411
DOI 10.1007/s11581-009-0354-0

ORIGINAL PAPER

NO_2 sensing properties of YSZ-based sensor using NiO and Cr-doped NiO sensing electrodes at high temperature

Perumal Elumalai · Jens Zosel · Ulrich Guth · Norio Miura

Received: 5 February 2009 / Revised: 3 April 2009 / Accepted: 11 May 2009 / Published online: 26 May 2009

Abstract Nickel oxide and chromium-doped nickel oxide ($Ni_{0.95}Cr_{0.03}O_{1-\delta}$) were prepared by thermal decomposition of nitrates. The obtained NiO and $Ni_{0.95}Cr_{0.03}O_{1-\delta}$ samples were utilized as sensing electrodes (SEs) in yttria-stabilized zirconia (YSZ)-based sensors for detection of NO_2 at 800 °C under wet condition (5 vol.% H_2O). While the mixed-potential-type planar sensor attached with NiO-SE gave rather large NO_2 sensitivity, the sensor attached with $Ni_{0.95}Cr_{0.03}O_{1-\delta}$-SE exhibited fast recovery rate with an acceptable sensitivity. The Δemf (electromotive force) of the sensors varied linearly with NO_2 concentration in the examined range of 50–400 ppm on a logarithmic scale. Based on the results of measurements for polarization, complex impedance and gas phase catalysis, the fast recovery was attributable to the high rate for the anodic reaction of O_2 at the $Ni_{0.95}Cr_{0.03}O_{1-\delta}$/YSZ interface, and the lower NO_2 sensitivity was caused by both the high rate for the anodic reaction of O_2 and the high degree for the gas phase conversion of NO_2 to NO.

P. Elumalai · N. Miura (✉)
Art, Science and Technology Center for Cooperative Research,
Kyushu University,
Kasuga-shi, Fukuoka 816-8580, Japan
e-mail: miurano@astec.kyushu-u.ac.jp

P. Elumalai
Japan Society for the Promotion of Science,
Tokyo 102-8471, Japan

J. Zosel · U. Guth
Kurt-Schwabe-Institute for Measuring and Sensor Technology,
Meinsberg, Germany

U. Guth
Institute of Physical Chemistry and Electrochemistry,
Dresden University of Technology,
Dresden, Germany

Keywords NO_x sensor · Mixed potential · YSZ · NiO · Chromium doping

Introduction

Demanding efforts towards the development of high-performance and reliable sensors for detection of toxic gases such as NO and NO_2 (known as NO_x), which are exhausted from automobiles, have been recently emphasized [1, 2] to meet the stringent emission regulations such as Tier 2 or Euro V (http://en.wikipedia.org/wiki/European_emission_standards). In automobile exhaust, along with NO_x, several other toxic components such as CO, hydrocarbons (HCs), and particulate matters (PMs) exist simultaneously, and the temperature goes up to even 900 °C during the acceleration of vehicles. Thus, a promising NO_x sensor should work well in such harsh conditions for a long time.

So far, yttria-stabilized zirconia (YSZ)-based mixed-potential-type NO_x sensors using oxide-based sensing electrodes (SEs) [3–16] are considered to be among the most promising devices in terms of their high sensitivity, lower cost, and portability. Moreover, they have definite linear relationship between the non-Nernstian potential and a logarithm of concentrations of a target gas in oxygen-containing atmosphere [6, 10, 13–15].

Recently, we have found that NiO can be used as an electrode material and its NO_2 sensing properties were attractive even at high temperature of above 800 °C [13, 14, 17]. To improve the NO_2 sensitivity of the sensor attached with NiO-SE, a second component, Rh or WO_3, was added to NiO and reported that the resulting NiO-based SE gave a large improvement of NO_2 sensitivity [18, 19]. The added Rh particles act as catalyst sites for cathodic reaction of

NO_2 and lead to high rate and thus high NO_2 sensitivity. In the case of WO_3-added NiO-SE, WO_3 was found to be completely evaporated from NiO matrix during sintering at 1400 °C, leading to increased porosity on NiO matrix (or lower degree for gas phase conversion of NO_2 to NO) and then to the increased NO_2 sensitivity.

Quite recently, the use of heterolayer consisting of Cr_2O_3 and NiO was reported to exhibit selective and sensitive response to NO_2 at high temperature [20]. It was considered that the Cr_2O_3 layer acts as a catalyst for the decomposition of reducible gases (CO, NO, and HCs) and then leads to selective NO_2 response. This interesting report motivated to investigate the sensing characteristics of Cr-doped NiO as a SE. Thus, Cr was doped in NiO and its NO_2 sensing performances were examined here and compared with pure NiO as well as with our previous results. Each of NiO and $Ni_{0.95}Cr_{0.03}O_{1-\delta}$ (representative composition) was synthesized by thermal decomposition of nitrates and followed by annealing at high temperature. As a result, it was found that the mixed-potential-type YSZ-based sensor attached with $Ni_{0.95}Cr_{0.03}O_{1-\delta}$-SE exhibited faster recovery rate with acceptable NO_2 sensitivity. The detailed process for synthesis, characterization, and NO_2 sensing properties are reported here.

Experimental

Synthesis and characterization of NiO and Cr-doped NiO

$Ni(NO_3)_2{\cdot}6H_2O$ or stoichiometric amounts of $Ni(NO_3)_2{\cdot}6H_2O$ and $Cr(NO_3)_3{\cdot}9H_2O$ for $Ni_{0.95}Cr_{0.03}O_{1-\delta}$ (this notation was used throughout the manuscript) were dissolved in distilled water, agitated with a magnetic stirrer, and evaporated on a hot plate. The precipitation was transferred into an alumina crucible and sintered in a chamber kiln in air at 800 °C for 5 h and at 1,400 °C (heating and cooling rates, 5 °C/min) for 2 h in air. The resulted powder was milled using ethanol and dried at 80 °C.

The crystal structure of NiO or $Ni_{0.95}Cr_{0.03}O_{1-\delta}$ samples was examined with an X-ray diffractometer (RIGAKU, RINT 2100VLR/PC). The CuKα radiation (λ = 1.5406 Å) and 0.5°/min angle step were used for all measurements. The surface morphology SE was observed using a field emission scanning electron microscopy (FE-SEM, JEOL, JSM-340F) operating at 15 kV. The composition of Cr and Ni was analyzed using an energy-dispersive X-ray analyzer (EDX, HORIBA, EX-220SE). The differential thermogram was obtained using simultaneous TG-DTA thermal analyzer (SETARAM Setsys TG-DTA 16).

The synthesized powders were cold-pressed into pellets 10 × 3 × (1–2) mm^3 with four Pt wires and sintered in air at 1,350 °C for 10 h. The electrical conductivity was measured by dc method in argon and oxygen gas mixtures.

Fabrication of sensor device

Commercially available YSZ plates (8 mol% Y_2O_3-doped, 10 × 10 mm, 0.2-mm thickness) were used for the fabrication of the planar sensors. The synthesized NiO or $Ni_{0.95}Cr_{0.03}O_{1-\delta}$ powder was thoroughly mixed with α-terpineol to obtain a paste. The obtained paste was applied on the front side of the YSZ plate attached with narrow Pt stripes (served as electron collector) by means of screen printing technique to make a SE. A commercial Pt paste (Tanaka Kikinzoku, TR 7907) was printed on the backside of YSZ plate as a reference electrode (RE). To make a good electrical contact with the measuring equipment, Pt wires (0.1 mm in diameter) were spot-welded using a Pt paste onto Pt connecting spots of both SE and RE. Each planar sensor obtained by that preparation was kept at 130 °C for 2 h in atmospheric air and was subsequently sintered at 1,400 °C for 2 h in air.

Evaluation of sensing performances and electrochemical properties

NO_x sensing characteristics were measured using a conventional gas flow apparatus equipped with a furnace operating in a temperature range of 800–900 °C. The sample gas containing various concentrations of NO_2 from 50 to 400 ppm was prepared by diluting a parent gas (505 ppm NO_2 in dry N_2) with dry N_2 and O_2. The base gas was composed of 5 vol.% O_2 and N_2 balance. Both the sample gas and the base gas were humidified with 5 vol.% (50,000 ppm) H_2O vapor by means of a water vapor generator coupled with a small evaporator and a micro-flow pump (Hitachi, L-2100). Both of the base gas and the sample gas were allowed to flow over the sensor at a constant flow rate of 100 cm^3/min. The volume of gas flow apparatus is about 50 cm^3. SE and RE were exposed simultaneously to the sample gas or the base gas. The potential difference [electromotive force (emf)] between SE and RE of the planar sensor was measured with a digital electrometer (Advantest, R8240) as a sensing signal. The SEs were always connected to the positive terminal of the electrometer.

The current–voltage (polarization) curves were measured by means of an automatic polarization system (Hakuto Denko, HZ-3000) based on potential sweep method at a scan rate of 2 mV/min using a two-electrode configuration at 800 °C in the base gas (5 vol.% O_2 + N_2 balance) and in the sample gas containing 200 ppm NO_2 (+5 vol.% O_2 + N_2 balance). The current axis of the anodic polarization curve was subtracted from that of the cathodic polarization curve

at each potential so as to obtain the modified polarization curve in which the current axis was expressed in absolute scale. The complex impedance measurements of the sensors were performed by means of a complex impedance analyzer (Solarton, 1255 WB) in the frequency range from 0.001 Hz to 1 MHz at 800 °C.

Measurements of NO_2 conversion to NO

The catalytic activity to the gas phase decomposition of NO_2 (100 ppm NO_2 + 5 vol.% O_2 + N_2 balance) to NO was evaluated for each of 1,400 °C-sintered NiO and $Ni_{0.95}Cr_{0.03}O_{1-\delta}$ samples (0.1 g each) using a conventional flow cell as well as a NO_x analyzer (Yanaco, ECL-88A) in the temperature range of 200–800 °C.

Results and discussion

Crystal structure of powder samples

Figure 1 shows the X-ray diffraction (XRD) patterns of as-prepared NiO and $Ni_{0.95}Cr_{0.03}O_{1-\delta}$ powders. The set of Bragg peaks in each pattern was indexed according to the standard XRD pattern, JCPDS PDF no. 47-1049. It is clearly seen that substitution of smaller Cr^{3+} ion (radius, 0.76 Å) in Ni^{2+} (radius, 0.83 Å) shift the position of Bragg peaks for Cr-doped NiO to higher angle (or lower 'd' spacing), which indicates the formation of solid solution. The estimated lattice parameter (a) values for NiO and $Ni_{0.95}Cr_{0.03}O_{1-\delta}$ samples were 4.154 and 4.141 Å, respectively. The crystallite sizes were calculated using Scherer formula and were found to be about 60 and 80 nm for NiO and $Ni_{0.95}Cr_{0.03}O_{1-\delta}$ samples, respectively. The XRD patterns of 1,400 °C-sintered NiO (not shown) or $Ni_{0.95}Cr_{0.03}O_{1-\delta}$ on YSZ plate showed also peaks for YSZ, besides the Bragg peaks for NiO or $Ni_{0.95}Cr_{0.03}O_{1-\delta}$. The formation of $Ni_{0.95}Cr_{0.03}O_{1-\delta}$ solid solution was substantiated from the results of differential thermal analysis (DTA). The DTA was performed on each of the as-prepared NiO and $Ni_{0.95}Cr_{0.03}O_{1-\delta}$ powders. The obtained results are shown in Fig. 2. The NiO sample shows an endothermic peak at around 290 °C due to phase transition from rhombohedral to cubic. It is seen that this endothermic peak disappears in $Ni_{0.95}Cr_{0.03}O_{1-\delta}$ sample. It means that Cr substitution stabilized NiO in cubic phase. Thus, it is likely that Cr is completely dissolved in NiO. The EDX analysis was performed on the $Ni_{0.95}Cr_{0.03}O_{1-\delta}$ sample to evaluate Ni and Cr contents. It was observed that the Ni and Cr metal contents were 49.0 and 1.8 at.%, respectively. Based on this, the estimated Ni [=Ni/(Ni + Cr)] and Cr [=Cr/(Ni + Cr)] compositions were 0.965 and 0.035, respectively, matching almost the nominal composition. Figure 3 shows the SEM images on the surface of $Ni_{0.95}Cr_{0.03}O_{1-\delta}$ sample. It can be seen that the average grain size is about 3 μm with narrow size distribution.

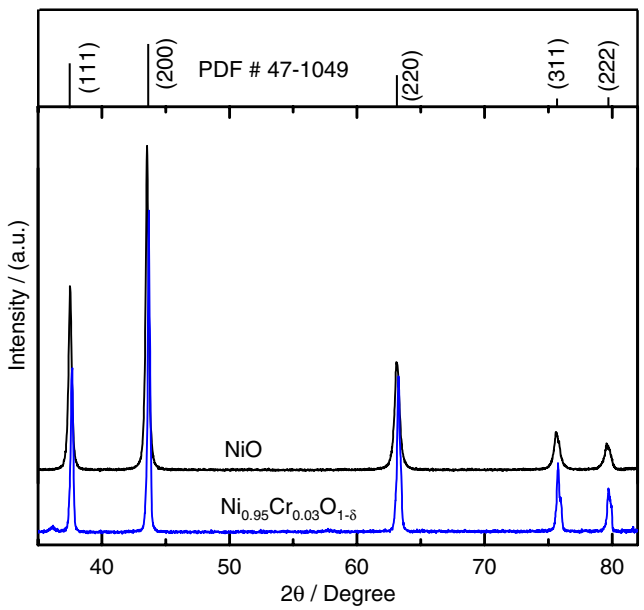

Fig. 1 X-ray diffraction patterns of as-prepared NiO (**a**) and $Ni_{0.95}Cr_{0.03}O_{1-\delta}$ (**b**)

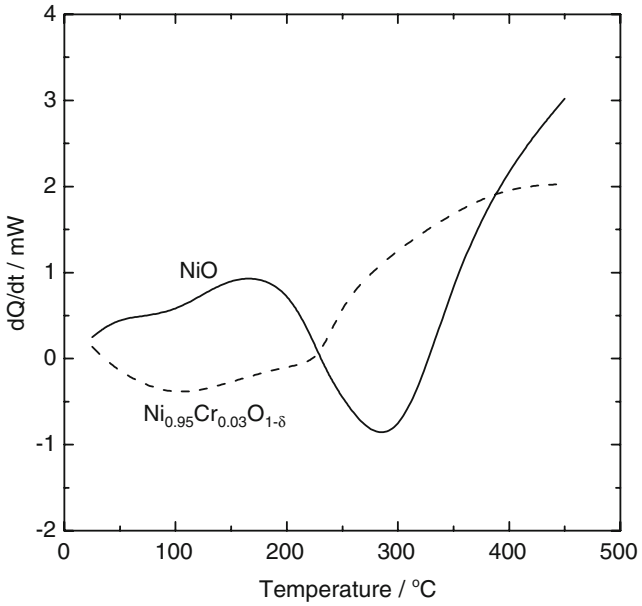

Fig. 2 Differential thermograms of NiO and $Ni_{0.95}Cr_{0.03}O_{1-\delta}$

The character of the conductivity of NiO is not changed by doping Cr within the temperature range of 400–700 °C. The conductivity increases with increasing oxygen partial pressure (p-type), as shown in Fig. 4. The conductivity of $Ni_{0.95}Cr_{0.03}O_{1-\delta}$ is slightly smaller than that of pure NiO. At temperatures higher than 700 °C, the activation energy

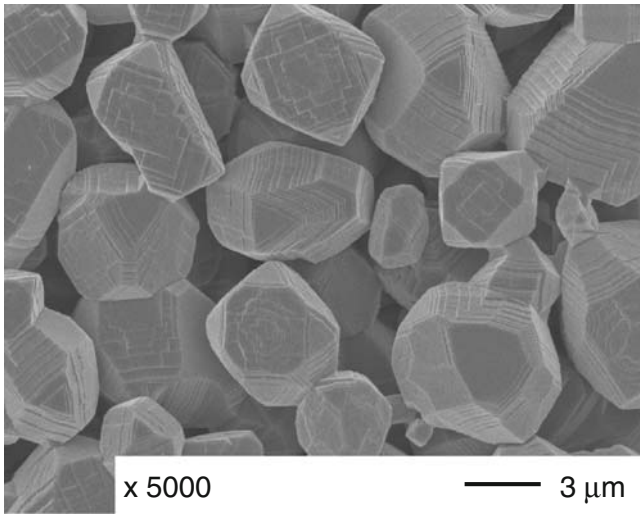

Fig. 3 SEM image on surface of 1,400 °C-sintered $Ni_{0.95}Cr_{0.03}O_{1-\delta}$ sample

for the conductivity becomes smaller, which suggests that a change in conductivity mechanism may be to the metallic.

Sensing properties of the planar sensors

The emf response to 200 ppm NO_2 was recorded at 800 °C for the planar sensors attached with each of NiO- and $Ni_{0.95}Cr_{0.03}O_{1-\delta}$-SEs under wet condition (5 vol.% H_2O). The obtained response transients are shown in Fig. 5. The emf values are close to zero under the base gas and change rapidly upon NO_2 flow and reach steady state within 2 min. The emf of both sensors returns to the base level in due time upon switching from the NO_2 to the base gas. It is seen that although the sensitivity of the sensor using NiO-SE is higher than that using $Ni_{0.95}Cr_{0.03}O_{1-\delta}$-SE, its recovery rate is rather slow. Undoubtedly, the sensor attached with $Ni_{0.95}Cr_{0.03}O_{1-\delta}$-SE exhibits faster recovery. The 90 % recovery times for the sensors attached with each of NiO- and $Ni_{0.95}Cr_{0.03}O_{1-\delta}$-SEs are approximately 210 s and approximately 50 s, respectively. This reveals that the recovery rate can be significantly enhanced by Cr doping in NiO.

The emf response transients to various concentrations of NO_2 were also recorded in the temperature range of 800–900 °C under the wet condition for the planar sensors attached with each of NiO- and $Ni_{0.95}Cr_{0.03}O_{1-\delta}$-SEs. Figure 6 shows the variation of sensitivity (Δemf) with the NO_2 concentration at different operating temperatures. The Δemf here is the difference between the emf of the sensor in the sample gas and that in the base gas. It is seen that in the both cases, the sensitivity varies linearly on the logarithm of NO_2 concentration in the examined range of 50–400 ppm at each operating temperature. Such linear dependence of sensitivity on the logarithm of NO_2 concentration is typical for a mixed-potential-type sensor [13–15]. It is seen that in both cases, the NO_2 sensitivity decreases with an increase in operating temperature of the sensors, and the sensitivity for the sensor using $Ni_{0.95}Cr_{0.03}O_{1-\delta}$-SE is lower in each operating temperature. Certainly, the highest NO_2 sensitivity could be achieved at lower operating temperature. The increase in operating temperature leads to faster kinetics (higher catalytic activity especially to anodic reaction of O_2) at SE/YSZ interface as well as to the degree of gas phase decomposition of NO_2 to NO on the surface of SE matrix. These two factors can lead

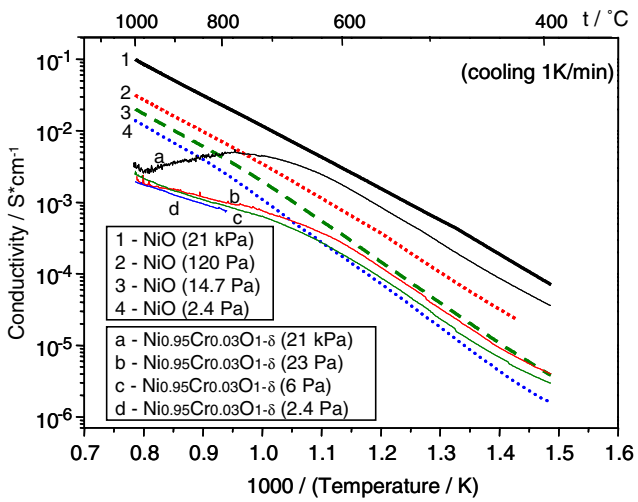

Fig. 4 Temperature dependence of conductivities of NiO and $Ni_{0.95}Cr_{0.03}O_{1-\delta}$ in various O_2 concentrations

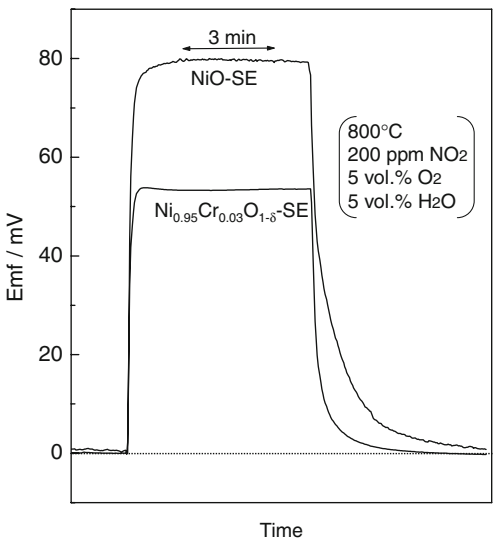

Fig. 5 Response transients to 200 ppm NO_2 at 800 °C for the planar sensors attached with NiO- and $Ni_{0.95}Cr_{0.03}O_{1-\delta}$-SEs under the wet condition (5 vol.% H_2O)

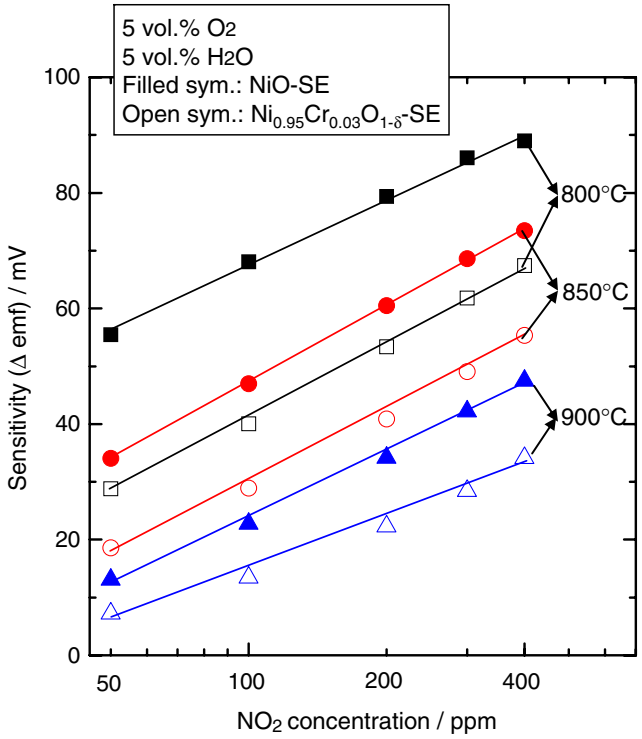

Fig. 6 Dependence of NO_2 sensitivity on the operating temperature of the planar sensors attached with NiO- and $Ni_{0.95}Cr_{0.03}O_{1-\delta}$-SEs under the wet condition

to lower NO_2 sensitivity at higher operating temperatures; higher rate of anodic reaction of O_2 leads to quicker recovery to the base level [13]. It is noted that the sensitivity of the present sensors attached with each of NiO- and $Ni_{0.95}Cr_{0.03}O_{1-\delta}$-SEs are better than those of the sensor attached with NiO-SE [13] and comparable with the sensor attached with heterolayer, Cr_2O_3/NiO (+ WO_3)-SE [20].

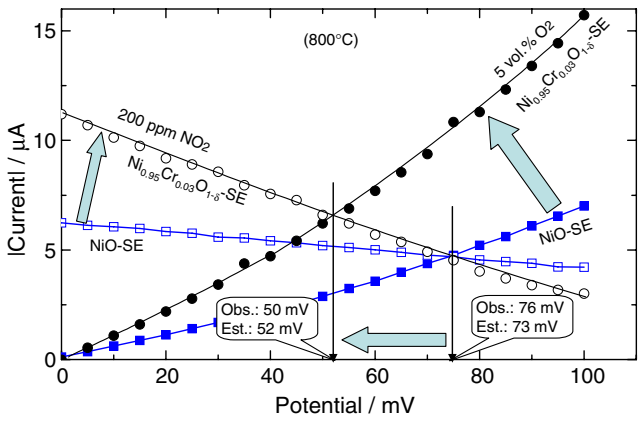

Fig. 7 Unmodified polarization curves in 5 vol.% O_2 (+ N_2 balance) and the modified polarization curves in 200 ppm NO_2 at 800 °C for the planar sensors attached with NiO- and $Ni_{0.95}Cr_{0.03}O_{1-\delta}$-SEs under the wet condition

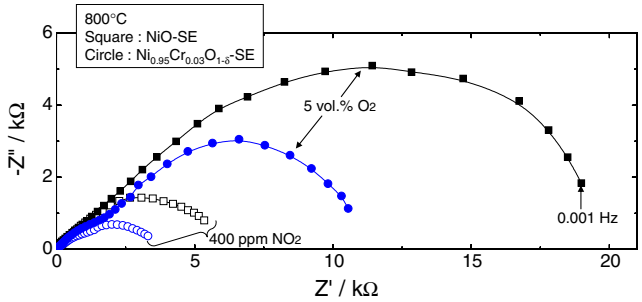

Fig. 8 Complex impedance plots in 5 vol.% O_2 (+ N_2 balance) and in 400 ppm NO_2 (+ base gas) at 800 °C for the planar sensors attached with NiO- and $Ni_{0.95}Cr_{0.03}O_{1-\delta}$-SEs under the wet condition

Verification of sensing mechanism

According to our previous reports and the aforesaid sensing properties, the sensing mechanism in the present case seems to be based on mixed-potential model [3, 13–15, 17–19]. When a SE is exposed to NO_2 in O_2-containing atmosphere, a non-Nernstian potential is developed on the SE due to the following two competitive electrochemical reactions:

$$O^{2-} \rightarrow 1/2O_2 + 2e^- (\text{anodic}) \quad (1)$$

$$NO_2 + 2e^- \rightarrow NO + O^{2-} (\text{cathodic}). \quad (2)$$

When the rates of reactions 1 and 2 are equal, a non-equilibrium potential (mixed potential) appears at the interface of SE/YSZ. Thus, to estimate the mixed potential and to examine the effect of Cr doping in NiO on the rates of the electrochemical reactions 1 and 2, the current–voltage (polarization) curves were measured at 800 °C in

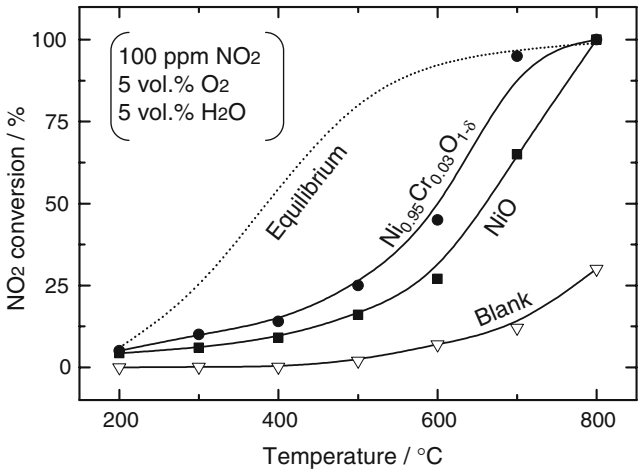

Fig. 9 Temperature dependence of NO_2 conversion to NO on 1,400 °C-sintered NiO and $Ni_{0.95}Cr_{0.03}O_{1-\delta}$ layers

the base gas (5 vol.% O_2 + N_2 balance) and in the sample gas containing 200 ppm NO_2 (+5 vol.% O_2 + N_2 balance) for the sensors attached with each of NiO- and $Ni_{0.95}Cr_{0.03}O_{1-\delta}$-SEs. The obtained polarization curves for anodic reaction of O_2 and the modified polarization curves for cathodic reaction of NO_2 are shown in Fig. 7 in which the current axis is expressed in an absolute scale. It is clear that both anodic as well as cathodic polarization curves for the sensor shifts upwardly when the SE was changed from NiO to $Ni_{0.95}Cr_{0.03}O_{1-\delta}$. This implies that the catalytic activity, especially for the anodic reaction of O_2 (1) is increased largely by Cr doping in NiO. Such a high rate for the anodic reaction of O_2 (1) leads to a faster recovery to the base level (Fig. 5) in the case of $Ni_{0.95}Cr_{0.03}O_{1-\delta}$-SE. As a result, the intersection between the anodic polarization curve and the cathodic polarization curve decreased from 73 to 52 mV when the SE of the sensors was changed from NiO to $Ni_{0.95}Cr_{0.03}O_{1-\delta}$. Evidently, these intersection values are in good agreement with the actual Δemf values of the sensor observed under potentiometric mode (Fig. 6). Such a close coincidence of the estimated and the observed values confirms that the sensing mechanism of the present sensor is based on mixed-potential model.

The increase in the catalytic activity to the cathodic reaction of NO_2 as well as to the anodic reaction of O_2 caused by the Cr doping in NiO was also substantiated by the results of measurements for complex impedances. Figure 8 shows Nyquist plots measured in the base gas and in the sample gas containing 400 ppm NO_2 (+5 vol.% O_2 + N_2 balance) for the sensors attached with each of NiO- and $Ni_{0.95}Cr_{0.03}O_{1-\delta}$-SEs at 800 °C under the wet condition. It is seen that in both cases, the impedance plots are in a form of a semicircle in the examined frequency range. It is worthy to note that the diameter of Nyquist plot in the base gas (or in the sample gas) for the sensor attached with $Ni_{0.95}Cr_{0.03}O_{1-\delta}$-SE is largely shrinking compared to that for the sensor attached with NiO-SE. This confirms that the rate of the anodic reaction of O_2 at the interface of $Ni_{0.95}Cr_{0.03}O_{1-\delta}$/YSZ is higher than that at the interface of NiO/YSZ. It is noted that although the conductivity of pure NiO sample (Fig. 4) is higher than that of $Ni_{0.95}Cr_{0.03}O_{1-\delta}$ sample, the charge transfer resistance (CTR) for the electrochemical reaction, i.e., the diameter of Nyquist plot, on NiO-SE is higher than that on $Ni_{0.95}Cr_{0.03}O_{1-\delta}$-SE. This is because the CTR is not related to the conductivity of SE material, but it is strongly dependent on the rate of electrochemical reactions 1 and 2.

To quantify the effect of Cr doping in NiO on the catalytic activity for the conversion of NO_2 to NO, which also plays an important role in deciding NO_2 sensitivity [13, 17], the degree of NO_2 conversion to NO was evaluated for NiO and $Ni_{0.95}Cr_{0.03}O_{1-\delta}$ samples sintered at 1,400 °C. The obtained results are shown in Fig. 9. It is quite interesting that $Ni_{0.95}Cr_{0.03}O_{1-\delta}$ exhibits higher catalytic activity of NO_2 decomposition reaction compared with NiO. This means that the concentration of NO_2 at the interface of $Ni_{0.95}Cr_{0.03}O_{1-\delta}$/YSZ is less than that at the interface of NiO/YSZ. Thus, such a high degree for the gas phase conversion of NO_2 to NO also contributes to low NO_2 sensitivity in the case of the sensor using $Ni_{0.95}Cr_{0.03}O_{1-\delta}$-SE.

It is noted that to evaluate the degree of gas phase NO_2 conversion to NO, we used powder samples. The observed degree of NO_2 conversion was as high as 99% at 800 °C. However, we feel that in the real sensing electrode, especially at the interface, the situation is not the same as that in the powder samples. Therefore, NO_2 is not completely decomposed to NO and still there exists NO_2. Thus, the sensors exhibited response to NO_2.

Based on the results obtained and discussed above, the Cr doping in NiO can give faster recovery with an acceptable NO_2 sensitivity. While the faster recovery can be attributable to the high rate for the anodic reaction of O_2, the lower NO_2 sensitivity was caused by both the high rate of anodic reaction of O_2 and the high degree for the gas phase conversion of NO_2 to NO.

Conclusions

The planar YSZ-based sensors were fabricated using each of NiO- and $Ni_{0.95}Cr_{0.03}O_{1-\delta}$-SEs and their NO_2 sensing properties were examined. The formation of $Ni_{0.95}Cr_{0.03}O_{1-\delta}$ solid solution was confirmed by the results of XRD and DTA measurements. Although the sensor attached with NiO-SE exhibited higher NO_2 sensitivity, the sensor attached with $Ni_{0.95}Cr_{0.03}O_{1-\delta}$-SE gave fast recovery rate with an acceptable sensitivity. The faster recovery and the lower sensitivity can be attributable to the higher rate for the anodic reaction of O_2 and the higher degree for the gas phase conversion of NO_2 to NO in the case of $Ni_{0.95}Cr_{0.03}O_{1-\delta}$-SE.

References

1. Docquier N, Candel S (2002) Prog Energy Combust Sci 28:107–150
2. Fergus JW (2007) Sens Actuat B Chem 121:652–663
3. Miura N, Kurosawa H, Hasei M, Lu G, Yamazoe N (1996) Solid State Ion 86–87:1069–1073
4. Hibino T, Ushiki K, Kuwahara Y (1997) Solid State Ion 93:309–314
5. Brosha EL, Mukundan R, Brown DR, Garzon FH (2002) Sens Actuat B Chem 87:47–57
6. Käding S, Jakobs S, Guth U (2003) Ionics 9:151–154
7. Szabo N, Dutta PK (2003) Sens Actuat B Chem 88:168–177

8. Martin LP, Pham AQ, Glass RS (2003) Sens Actuat B Chem 96:53–60
9. Ono T, Hasei M, Kunimoto A, Miura N (2004) Solid State Ion 75:503–506
10. Guth U, Zosel J (2004) Ionics 10:366–377
11. West DL, Montgomery FC, Armstrong TR (2005) Sens Actuat B Chem 111–112:84–90
12. Li X, Xiong W, Kale GM (2005) Electrochem Solid-State Lett 8: H27–H30
13. Elumalai P, Wang J, Zhuiykov S, Terada D, Hasei M, Miura N (2005) J Electrochem Soc 152:H95–H101
14. Elumalai P, Miura N (2005) Solid State Ion 176:2517–2522
15. Plashnitsa VV, Ueda T, Elumalai P, Kawaguchi T, Miura N (2008) Ionics 14:15–25
16. Zosel J, Franke D, Ahlborn K, Gerlach F, Vashook V, Guth U (2008) Solid State Ion 179:1628–1631
17. Elumalai P, Plashnitsa VV, Ueda T, Hasei M, Miura N (2006) Ionics 12:331–337
18. Wang J, Elumalai P, Terada D, Hasei M, Miura N (2006) Solid State Ion 177:2305–2311
19. Miura N, Wang J, Elumalai P, Ueda T, Terada D, Hasei M (2007) J Electrochem Soc 154:J246–J252
20. Elumalai P, Plashnitsa VV, Ueda T, Miura N (2008) Electrochem Commun 10:745–748